# Inhibition-Dominated Rich-Club Shapes Dynamics in Cortical Microcircuits in Awake Behaving Mice

[†]Hadi Hafizi[1], [†]Sunny Nigam[2*], Josh Barnathan[3], Naixin Ren[4], Ian H Stevenson[4,5], Sotiris C Masmanidis[6], Ehren L Newman[1], Olaf Sporns[1,7], and John M Beggs[3*]

[1]Department of Psychological and Brain Sciences, Indiana University, Bloomington, Indiana, USA
[2]Department of Neurobiology and Anatomy, McGovern Medical School, University of Texas, Houston, Texas, USA
[3]Department of Physics, Indiana University, Bloomington, Indiana, USA
[4]Department of Psychological Sciences, University of Connecticut, Storrs, Connecticut, USA
[5]Department of Biomedical Engineering, University of Connecticut, Storrs, Connecticut, USA
[6]Department of Neurobiology, David Geffen School of Medicine, University of California, Los Angeles, California, USA
[7]Indiana University Network Science Institute, Indiana University, Bloomington, Indiana, USA

[†]These authors contributed equally
*Correspondence: sunny.nigam@uth.tmc.edu, jmbeggs@indiana.edu

## SUMMARY

Functional networks of cortical neurons contain highly interconnected hubs, forming a rich-club structure. However, the cell type composition within this distinct subnetwork and how it influences large-scale network dynamics is unclear. Using spontaneous activity recorded from hundreds of cortical neurons in orbitofrontal cortex of awake behaving mice we show that the rich-club is disproportionately composed of inhibitory neurons, and that inhibitory neurons within the rich-club are significantly more synchronous than other neurons. At the population level, Granger causality showed that neurons in the rich-club are the dominant drivers of overall population activity and do so in a frequency-specific manner. Moreover, early activity of inhibitory neurons, along with excitatory neurons within the rich-club, synergistically predicts the duration of neuronal cascades. Together, these results reveal an unexpected role of a highly connected core of inhibitory neurons in driving and sustaining activity in local cortical networks.

## INTRODUCTION

Connectivity in brains is far from egalitarian. Some regions in the human cortex send and receive fiber bundles at a density ten times greater than others (Hagmann et al., 2008; Markov et al., 2013); the top 20% of cortical neurons in mouse carry 70% of the information flow (Nigam et al., 2016); the nervous system of the worm C. elegans contains a small number of well-connected neurons (Towlson et al., 2013). Even less democratic is the finding that in each of these systems, the most highly connected units (cortical regions, hub neurons) connect to each other more than expected by chance, forming what is called a rich-club structure (Dann et al., 2016; van den Heuvel and Sporns, 2011; Nigam et al., 2016; Towlson et al., 2013). Despite the ubiquity of the rich-club network structure across different species, the cell type composition within this distinct subnetwork and how it shapes network dynamics is unknown.

In the past decade, the relationship between neuron types and network structure has received increased research attention. In the developing hippocampus, hub neurons are all inhibitory (Bonifazi et al., 2009); more recent work in mouse somato-motor cortex slices found inhibitory neurons were more topologically central within networks than excitatory neurons (Kajiwara et al., 2021). However, neither of these studies directly examined the rich club and its cell type composition. It is unknown whether the rich-club is composed of entirely excitatory neurons, or if its composition corresponds to typically reported values (85%) of excitatory neurons in cortical networks/cortex (Douglas and Martin, 2004). More importantly, the influence of the rich-club on dynamics in local cortical networks is poorly understood. Recordings from multiple motor areas in behaving monkeys showed that the most highly connected rich-club neurons, which spanned these areas, were synchronous in beta and low frequency bands (Dann et al., 2016). Synchrony is thought to be a mechanism for forming assemblies of neurons and for coordinating switching between them (Cho et al., 2020; Fries, 2005; Tort et al., 2007). Recent modeling studies suggest that the rich-club could initiate and sustain cortical activity (Aguilar-Velázquez and Guzmán-Vargas, 2019; Gu et al., 2019), but this has not been experimentally observed yet.

We investigated these issues by analyzing dense electrode array recordings from the orbitofrontal cortex of awake behaving mice where the rich-club had been previously reported (Nigam et al., 2016). We found that the proportion of inhibitory neurons within the rich-club was significantly higher than previously reported values in cortical networks. Inhibitory neurons within the rich-club were more synchronous compared to other cell types found within and outside the rich-club. In addition, Granger causality analysis revealed that the rich-club drives spontaneous network activity in the rest of the network at low frequencies (< 10Hz). Finally, early activity of excitatory and inhibitory neurons in the rich-club synergistically predicted the lengths of neuronal cascades. Together, these findings reveal that inhibitory neurons within the rich-club play a central role in shaping dynamics in local cortical networks. Portions of this work were previously presented in thesis form (Hafizi, 2020).

## RESULTS

### High concentration of inhibitory neurons within the rich-club

Spike trains were recorded from awake mice (n = 990 neurons; N = 7 mice) with silicon microprobes placed in orbitofrontal cortex (Shobe et al., 2015) (Figure 1A). We limited our analysis to portions of the data when the mice were not involved in a task and were immobile on

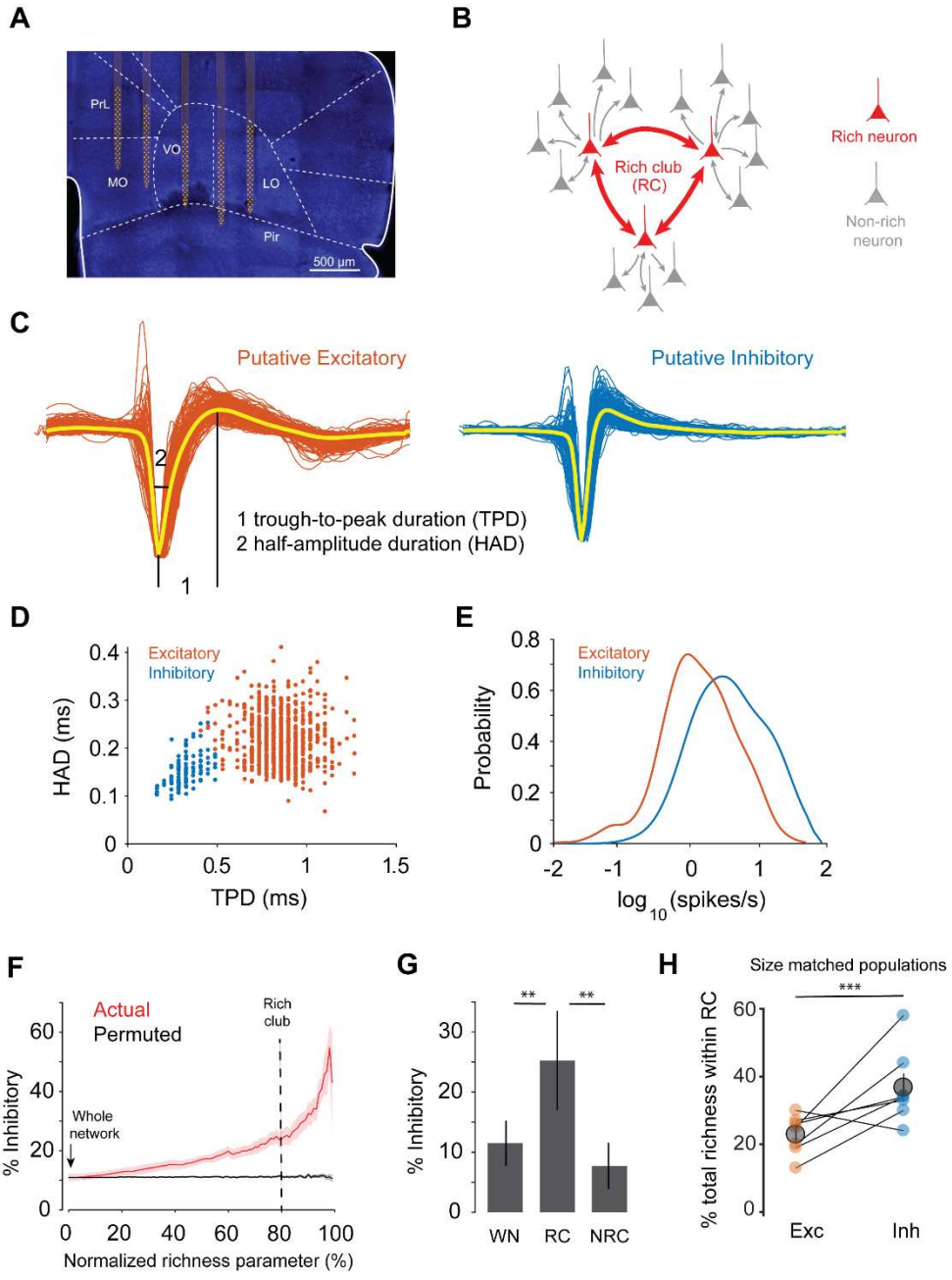


**Figure 1. Unexpectedly high concentration of inhibitory neurons in the rich-club. (A)** Spatial position of 5 silicon microprobes (256 electrodes in total) spanning medial to lateral orbitofrontal cortex in awake head-fixed mice. **(B)** Schematic of the rich-club organization in neuronal networks, illustrating a few hub neurons (red) forming a dense and strongly connected subnetwork within themselves (red) and surrounded by a larger community of neurons (non-rich sub network) with fewer and weaker connections (gray). Thickness of the lines represent connection strength. **(C)** Spike waveforms of putative excitatory (orange) and inhibitory (blue) neurons from a representative session with trough-to-peak and half-amplitude duration marked; note the significant difference of spike width between the two putative cell types. **(D)** Scatter plot of spike waveform features from (C) showing two distinct clusters of neurons. ® Firing rate distributions of putative inhibitory and excitatory neurons from the same session as in C-E. **(F)** Percentage of putative inhibitory neurons (averaged across N = 7 sessions) in subnetworks as a function of the normalized richness parameter ® (red) and for size matched networks with randomly permuted labels for excitatory and inhibitory neurons (gray; N = 100 permutations per data set). Solid curves represent the mean and shaded areas represent s.e.m. over all

data sets. **(G)** Percentage of inhibitory neurons in the whole network (WN), within the rich-club (RC) and the non-rich club (NRC). Asterisks denote statistical significance (single-tailed Wilcoxon signed-rank test; $P < 0.05$). **(H)** Proportion of total richness (incoming TE + outgoing TE) accounted for by inhibitory neurons and size matched population of excitatory neurons within the rich-club. Asterisks denote statistical significance (Wilcoxon signed-rank test; $P < 0.001$).

the treadmill (see Methods). We used Transfer Entropy (TE) to construct effective connectivity networks (weighted and directed graphs) between hundreds of neurons in each session. These networks were found to contain a distinct subnetwork of hub neurons (high incoming and outgoing TE connections) with a higher than expected density and strength of connections between them forming a rich-club (Figure 1B) (Nigam et al., 2016). Neurons outside the rich-club formed the non-rich subnetwork characterized by fewer and weaker connections.

To examine the cell-type composition of these distinct subnetworks we used spike waveform features (trough-to-peak duration and half amplitude duration) and firing rates to classify neurons as putative excitatory or inhibitory neurons (Ren et al., 2020) (see Methods) (Figure 1C). Using this classification scheme, we were able to assign putative cell types to 97% of the recorded neurons and the different cell types formed clearly separable clusters in feature space (Figure 1D) with distinct firing rate distributions for both cell types (Figure 1E). Next, we isolated sub-groups of neurons whose normalized richness parameter (sum of incoming and outgoing TE) was higher than a certain threshold and calculated the percentage of inhibitory neurons within those sub-networks. We observed a steady increase of the percentage of inhibitory neurons within subnetworks as we increased the threshold richness parameter value, ranging from 11% in the whole network to as high as 55% in the richest subnetworks (Figure 1F). We calculated chance levels of the percentage of inhibitory neurons in size matched sub-networks with the same TE values, by randomly permuting the identity of cell types throughout the network. Contrary to the actual networks with preserved cell identities, the percentage of inhibitory neurons was roughly uniform across the range of the richness parameter. Our findings reveal the highly non-random embedding of specific cell-types in these cortical networks. Throughout the rest of the paper, we will take the 80% line in Figure 1F to be representative of the rich-club, although in fact the range of the rich-club is larger than that and extends from 5% to 100%. Our results do not qualitatively differ if we change this threshold by ± 10%, consistent with our previous work (Nigam et al., 2016). With this threshold, the percentage of inhibitory neurons within the rich-club ($25 \pm 8\%$) was significantly higher (single-tailed Wilcoxon signed-rank test, $P < 0.005$) compared to that in the non-rich subnetwork ($7.7 \pm 4\%$) or in the whole network ($11.5 \pm 4\%$) (Figure 1G). Additionally, within the rich-club, size matched populations of excitatory neurons accounted for significantly lower total richness ($22 \pm 2\%$) compared to inhibitory neurons ($37 \pm 4\%$; Wilcoxon signed-rank test; $P < 0.001$) (Figure 1H). Hence, although inhibitory neurons constitute roughly 25% of the neurons within the rich-club they account for significantly higher richness per-capita compared to excitatory neurons.

## A highly synchronous group of inhibitory neurons within the rich-club

Given that inhibitory neurons are often implicated in synchrony (Bush and Sejnowski, 1996; Hasenstaub et al., 2005; Van Vreeswijk et al., 1994), we next sought to investigate whether the spiking dynamics within the rich subnetwork showed more synchrony than in the rest of the network. To quantify synchrony, we calculated the shuffle corrected Normalized Cross-Correlation Histograms (NCCH) of pairs of neurons within and across these subnetworks (see

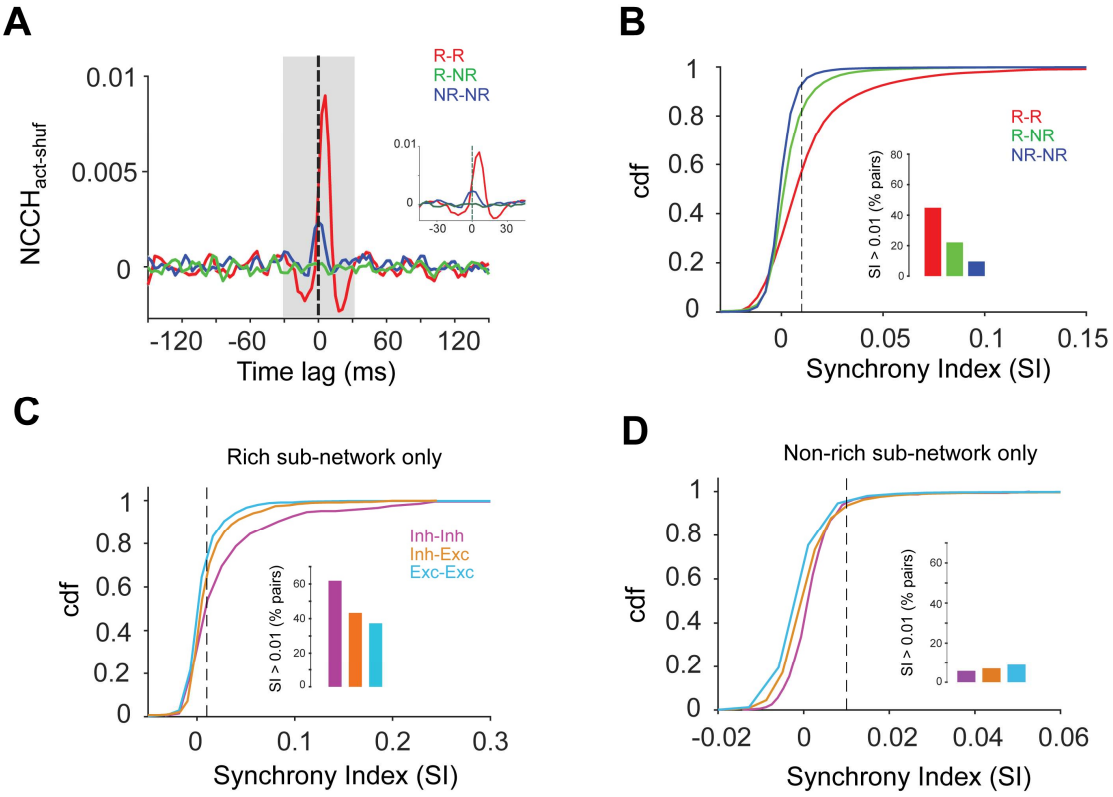


**Figure 2. Inhibition dominates higher pairwise synchrony within the rich-club subnetwork. (A)** Representative examples of shuffle corrected normalized cross-correlation histograms (NCCH) evaluated at different time lags (+120 to -120 ms) for a pair containing neurons only within the rich-club subnetwork (red), only within the non-rich subnetwork (blue) and a pair with mixed membership (green). Gray shaded region represents time window used for the calculation of Synchrony Index (SI). Inset shows a zoomed in version of the same NCCH between ± 45 ms. Note sharply peaked synchronous activity for the pair involving rich neurons compared to other pairs. **(B)** Cumulative distribution of SI across all sessions (N = 7) for pairs containing neurons only within the rich-club (red; N = 2958 pairs), only within the non-rich subnetwork (blue; N = 46357 pairs) and pairs constituting neurons with mixed membership (green; N = 23913 pairs). Inset shows percentage of pairs in each group that have SI values greater than 0.01. **(C)** Cumulative distribution functions of synchrony index only within the rich-club for inhibitory-inhibitory (purple; N = 207 pairs), inhibitory-excitatory (orange; N = 1135 pairs) and excitatory-excitatory pairs (cyan; N = 1465 pairs). Inset shows percentage of pairs for each cell type combination that have SI values greater than 0.01. **(D)** Same as in C except for pairs within the non-rich subnetwork. Note unlike differences seen within the rich-club, no significant difference between cell types is observed within the non-rich subnetwork (2 sample KS test; P > 0.1). Inset shows percentage of pairs for each cell type combination that have SI values greater than 0.01.

Methods). Figure 2A shows representative examples of NCCH of pairs belonging to the different subnetworks. The example pair within the rich-club exhibits a higher level of coordinated activity compared to pairs within the non-rich subnetwork or pairs with mixed membership. To quantify

this, for each pair we calculated the area under the NCCH curve between ± 30 ms and defined it to be the Synchrony Index (SI). The cumulative distribution of SI (Figure 2B) for all pairs (N = 2958) within the rich subnetwork was significantly different from that of the pairs within the non-rich subnetwork (N = 46357) or pairs with mixed membership (N = 23913) (Figure 2B; two sample KS test; $P < 0.01$; see Supplementary Figure S1 for cumulative distribution for each session) with higher mean values of SI within the rich-club compared to other subnetworks ($\langle SI_{rich-rich} \rangle = 0.016$; $\langle SI_{rich-nonrich} \rangle = 0.005$; $\langle SI_{nonrich-nonrich} \rangle = 0.002$). In fact, close to 45% of the pairs within the rich-club had SI values greater than 0.01, whereas only 22% and 9% of non-rich and inter-network pairs were above this threshold respectively (Figure 2B inset). Hence, pairs within the rich subnetwork exhibit higher synchrony compared to that observed outside the subnetwork.

To examine whether this higher synchrony within the rich-club was cell type specific, we grouped SI values for pairs within the rich-club into three classes: pairs where both neurons were inhibitory (N = 207), both neurons were excitatory, (N = 1135) and pairs with a mixed membership (excitatory and inhibitory; N = 1465). The cumulative distribution function of the SI values (Figure 2C; see Supplementary Figure S2 for cumulative distribution for each session) for pairs involving inhibitory neurons only was significantly different from that of inhibitory-excitatory pairs or excitatory-excitatory pairs (two-sample KS test; $P < 0.01$) with higher mean values of SI between inhibitory pairs ($\langle SI_{inh-in} \rangle = 0.04$; $\langle SI_{inh-exc} \rangle = 0.02$; $\langle SI_{exc-exc} \rangle = 0.01$). In fact, close to 60% of the inhibitory pairs within the rich-club had SI values greater than 0.01, whereas only 42% and 36% of the rest of the cell pairs in the other groups were above this threshold (Figure 2C inset). Thus, within the rich subnetwork, inhibitory neurons exhibited higher pairwise synchrony compared to other classes of pairs. To examine whether this higher synchrony was simply a characteristic of cell type, we looked at the cumulative distributions of SI within the non-rich subnetwork for the different classes of pairs (Figure 2D; see Supplementary Figure S3 for cumulative distribution for each session). Surprisingly, we found no significant difference between the cumulative SI distributions (two sample KS test; $P > 0.1$) for the different classes of pairs within the non-rich subnetwork. Moreover, the mean SI for the different classes ($\langle SI_{inh-} \rangle = 0.002$; $\langle SI_{inh-exc} \rangle = 0.002$; $\langle SI_{exc-exc} \rangle = 0.002$) within the non-rich subnetwork were an order of magnitude smaller than that within the rich-club with less than 10% of pairs of any class having SI values > 0.01. Our results show that only inhibitory neurons within the rich subnetwork are characterized by higher synchrony, highlighting the role of network topology in shaping the dynamics of specific cell types.

**Rich-club drives network dynamics**

Given that synchrony has been implicated in enhancing the efficacy of a signal (Bosman et al., 2012; Womelsdorf et al., 2007), and that network structure influences dynamics (Chambers and MacLean, 2016), we next sought to investigate if this enhanced synchrony within the rich-club influenced activity in the rest of the network. Neurons within either sub-network (rich or non-rich) could trigger activity in the other through functional connections (Figure 3A). To examine this, we

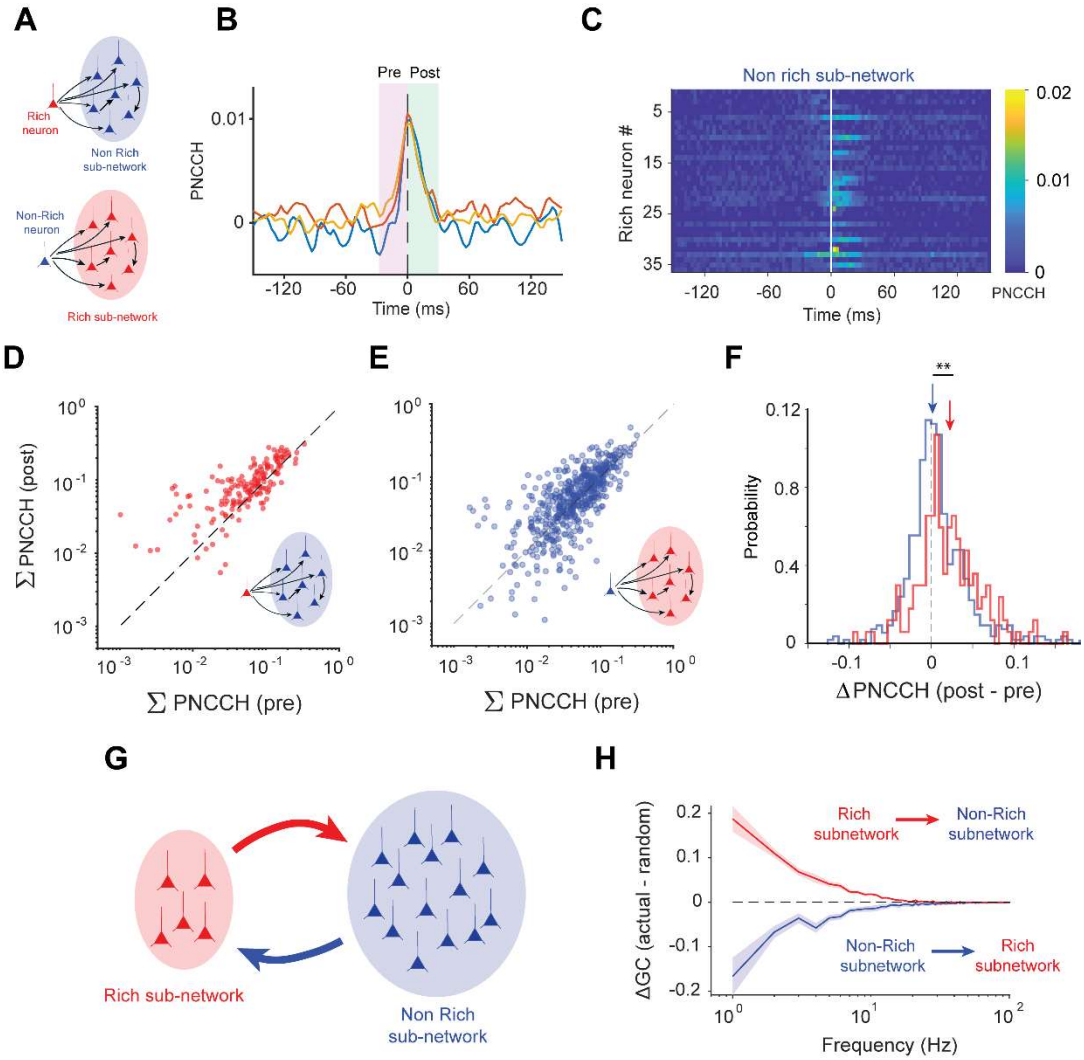


**Figure 3. Rich-club neurons drive network activity in cortical microcircuits. (A)** Schematic representation of how single neurons within the rich/non-rich subnetworks can influence activity in the other subnetworks through functional interactions. **(B)** Example population normalized cross-correlation histogram (PNCCH) for three rich neurons evaluated for a range of time lags. Shaded regions represent time windows pre- and post-spiking used for further analysis. **(C)** Representative PNCCH for all rich neurons from an example session. Horizontal rows in the heat map represent the PNCCH between a particular rich neuron and the population activity of non-rich neurons calculated at different time lags (-150 to +150ms) (see Methods). Note higher values of PNCCH post-spiking of a rich neuron compared to pre-spiking. **(D)** Summed post (0 to +30 ms) and pre PNCCH (-30 to 0 ms) values for all rich neurons across all 7 sessions (red filled circles; N = 188 neurons). The reference population used for calculating the PNCCH was the non-rich subnetwork. **(E)** Same as in (D) except PNCCHs are evaluated between the spiking activity of one non-rich neuron and the rich neuron sub-population (N = 435 neurons). Each red and blue dot represents a single neuron **(F)** Distribution of the difference in summed PNCCH values pre- and post-spiking for rich neurons (red) and non-rich neurons (blue). Blue and red arrows represent the median values of each distribution (asterisk denote statistical significance of a Wilcoxon rank-sum test; $P<0.001$). **(G)** Schematic of how overall population activity in each subnetwork can drive activity in the other through functional interactions. **(H)** Difference of Granger causality values between actual and size matched randomly sampled networks as a function of frequency from the rich-club to the non-rich subnetwork (red) and vice versa (blue). Solid lines represent mean values across N = 7 sessions and shaded regions represent s.e.m.

calculated the Population Normalized Cross-Correlation histogram (PNCCH; see Methods) between the spike times of a single rich/non-rich neuron and the combined spike times of the rest

of the rich/rich neurons respectively at multiple time lags extending from -150 to +150 ms. Figure 3B shows representative examples of PNCCH evaluated for the spiking activity of three rich neurons and the non-rich subnetwork. Heatmaps of PNCCH for all rich neurons from an example session show higher correlated activity post spiking of a rich neuron compared to pre-spiking. (Figure 3C). To quantify this further, we calculated the pre-spiking area under the PNCCH curve between -30 to 0ms and the post-spiking area between 0 to 30 ms (Figure 3B, shaded regions). A population wide analysis showed that post PNCCH values were significantly higher compared to pre PNCCH values in case of both the rich (Figure 3D) as well as the non-rich neurons (Figure 3E) ($P < 0.01$, Wilcoxon signed-rank test). However, the difference between post and pre values ($\Delta$PNCCH) was significantly higher for the rich neurons compared to the non-rich neurons (Figure 3F) (Wilcoxon rank-sum test; $P < 0.001$). Our results indicate that there is an asymmetry in single cell and network interactions where neurons within the rich-club lead non-rich neurons.

To further analyze the strength and directionality of the interactions between the rich and non-rich subnetworks at the scale of neuronal populations, we estimated Granger causality (GC) from the rich to non-rich and non-rich to rich subnetworks using the population spiking activity in these sub-populations. To specifically examine the role of network topology, we randomly sampled neurons from the entire network to create size matched pseudo rich and non-rich subnetworks and calculated GC values between such subnetworks. We subtracted these values from the estimate of GC between the actual rich/non-rich subnetworks. This revealed we found higher than expected GC from the rich to non-rich and less than expected GC from non-rich to rich subnetwork at low frequencies ($\leq$10 Hz) (Figure 3H). Our results suggest that network topology endows the rich-club with a greater capability to drive network activity in other parts of the network.

**Participation of inhibitory and excitatory neurons at early stages synergistically predicts the length of neuronal cascades**

Motivated by the fact that the rich-club drives activity at the population level, we sought to examine if this was also the case neuronal cascades. Previous work with multielectrode array recordings (Beggs and Plenz, 2003) defined a neuronal cascade as continuous spiking activity spanning one or more time bins, bracketed by time bins of no activity at the beginning and at the end (Figure 4A). The number of consecutive time bins with at least one active neuron is defined as the cascade length (CL; see Methods). These cascades are known to have lengths that exceed what would be expected from randomly shuffled data (Figure 4B) (Beggs and Plenz, 2003, 2004). Because synchrony has been suggested to enhance signal propagation (Fries, 2005), we wondered if increased synchrony could also be related to cascade length (CL). Indeed, we found that there was a statistically significant relationship such that longer cascades were characterized by greater amounts of synchrony (Supplementary Figure S4). To investigate how cell types within the rich/non-rich subnetwork contributed to this, we plotted the fraction of neurons that participated in cascades of different lengths. We looked at four categories of neurons: excitatory and inhibitory neurons within the rich-club; and excitatory and inhibitory neurons in the non-rich subnetwork. Our analysis revealed that the participation of inhibitory neurons in the rich-club increased with cascade length (Figure 4C). Interestingly, the participation of excitatory neurons not in the rich-club decreased with cascade length (Figure 4F). No relationship was found between cascade

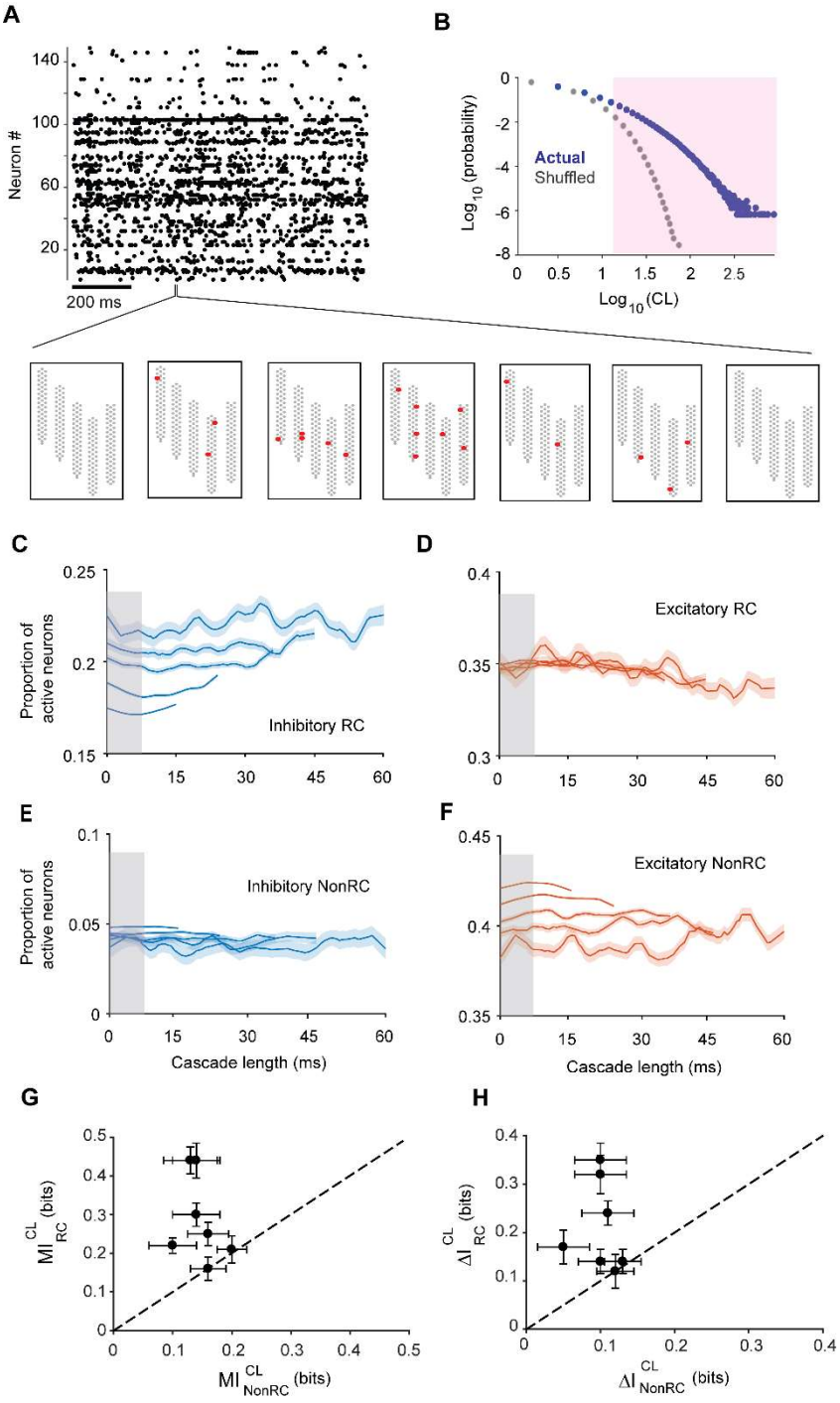


**Figure 4. Participation of inhibitory and excitatory neurons at early stages synergistically predicts cascade length. (A)** Example spike raster of simultaneously recorded neurons (N = 142) from an example session (top). Representative example of a neuronal cascade: a spatiotemporal sequence of neuronal activity with at least one active neuron per time bin, flanked by time-bins with no activity (bottom). Gray dots represent electrode locations on the silicon probe and red dots represent active single units at each time step of the cascade. **(B)** Distribution of cascade length (CL) in actual (blue) and shuffled data (grey) for the same session as in (A). Shaded area represents the region where distribution of cascade lengths in the actual data (blue dots) significantly differs from that expected by chance (gray dots). **(C)** Percentage of active inhibitory neurons within the rich-club at different time bins of cascades of different lengths. **(D)** Same as in (C) except for active excitatory neurons. Note that participation of excitatory neurons

stays constant along different cascades whereas inhibitory neurons' participation increases with the length of the cascade. **(E, F)** Same as in (C) and (D) except for the percentage of active excitatory and inhibitory neurons within the non-rich subnetwork. **(G)** Mutual information between cascade lengths and percentage of active excitatory and inhibitory neurons within and outside the rich-club (y and x axis respectively) in the first 3 time-bins (gray shaded region in C-F) in each of the 7 sessions. **(H)** ΔI values (difference between joint MI and independent sum; see Methods) for each of the 7 sessions. Error bars in G, H represent s.e.m.

lengths and the participation of excitatory neurons in the rich-club or inhibitory neurons not in the rich-club (Figure 4D, E).

Because the level of participation of inhibitory neurons within the rich-club and excitatory neurons outside the rich-club at the outset of a cascade seemed to be related to cascade length, we examined if the activity among these neurons in the first three time steps could predict cascade length. We quantified this relationship by calculating mutual information using the Information Breakdown toolbox (Magri et al., 2009a) (see Methods). We calculated the bias corrected joint mutual information between the percentage of active neurons (excitatory and inhibitory) in the first three bins of the cascades and the lengths of the cascades. Indeed, we found significant mutual information encoded in the joint percentage activation of both cell types about cascade length in all 7 sessions both in the rich and the non-rich subnetworks (Figure 4G). Five out of the 7 sessions showed significantly higher mutual information within the rich-club compared to that in the non-rich subnetwork (Wilcoxon's rank-sum test; $P < 0.001$) indicating a significant role played by the rich-club in determining cascade dynamics. Additionally, we examined whether the sum of the information encoded separately in the percentage activations of excitatory and inhibitory neurons was lower or exceeded the joint mutual information (see Methods). We found that not only was the information in the percentage activations synergistic ($\Delta I > 0$; signed-rank test, $P < 0.001$) in both rich and non-rich subnetworks but that the rich subnetwork had significantly higher synergy compared to the non-rich subnetwork (Figure 4H; Wilcoxon signed-rank test, $P < 0.001$). Our results indicate that the early activation profile of inhibitory neurons along with that of excitatory neurons jointly encode information in a synergistic manner about cascade dynamics.

## Discussion

The dynamics in networks of cortical neurons is expected to be strongly influenced by their pattern of connections and their cell type composition. Here we show that within subnetworks consisting of highly connected hub neurons (rich-club) inhibitory to excitatory ratio is significantly higher compared to the entire network or the non-rich subnetwork. Inhibitory neurons within the rich-club exhibit higher pairwise synchrony compared to other pairs within and outside the rich-club. This distinct subnetwork may also play a dominant role in causally shaping network dynamics in a frequency specific manner. Interestingly, early activation of inhibitory neurons along with excitatory neurons within the rich-club synergistically determine the length of spatiotemporal patterns of activity. Our findings provide a novel perspective on how cell type (excitatory vs inhibitory) coupled with a non-random network topology (highly connected rich-club) plays a central role in regulating network dynamics in cortical microcircuits.

**Relation to previous work.** Previous studies in the hippocampus have shown the existence of densely connected neuronal hubs. Notably, these hubs were found to be GABAergic interneurons rather than excitatory neurons (Bonifazi et al., 2009; Picardo et al., 2011). These hub neurons shared strong connections with nearby pyramidal neurons (English et al., 2017) and played a crucial role in regulating overall network synchronization (Bonifazi et al., 2009). Moreover, hub

neurons maintained their connectivity profile from development to adulthood highlighting the importance of this network topology throughout the lifetime of the animal (Bocchio et al., 2020). In the developing barrel cortex GABAergic neurons have been shown to form functional assemblies that evolve during post-natal development with sensory stimulation. (Modol et al., 2020). Kajiwara and colleagues (Kajiwara et al., 2021) found that inhibitory neurons were more centrally located within the functional network topology of somato-motor cortex in mouse slices. However, a broader characterization of functional connectivity in cortical circuits is lacking, especially in a higher cortical area such as the orbitofrontal cortex. Here, our findings reveal the existence of a densely connected rich-club with a higher percentage of inhibitory neurons compared to the rest of the network. Rich-club neurons appear to play a pivotal role in regulating network dynamics. Only inhibitory neurons within the rich-club had higher levels of synchrony and were better predictors of the duration of spatiotemporal patterns compared to inhibitory neurons outside the rich-club. Hence network topology determines the contribution of specific cell types to network dynamics.

We have shown how specialized subnetworks i.e., rich-clubs with a higher inhibitory to excitatory ratio, regulate network dynamics of spontaneous activity in cortical microcircuits. However, the role of this distinct subnetwork in representing sensory information or task related variables in cortical networks is unknown. Specifically, do these subnetworks have a greater capacity of encoding or decoding sensory/task specific information? Previous work in cortical columns in macaque V1 has shown the presence of synergy hubs i.e., certain neurons that engage in predominantly synergistic interactions with other neurons to encode stimulus information (Nigam et al., 2019). Interestingly, sub-populations consisting of only synergy hubs were better at decoding stimulus information compared to redundancy hubs. However, the cell type composition of synergy hubs and whether they form a densely connected rich-club is unknown. Additionally, recent work in cortical slice cultures have shown that neurons with the highest synergy values tend to reside in the rich-club (Faber et al., 2019). Future work in sensory as well as non-sensory cortical areas can examine this missing link between network topology and information encoding in neuronal populations.

**Inhibition driven network activity:** We observed higher participation of inhibitory neurons within the rich-club in longer spatiotemporal patterns. It would seem paradoxical that inhibitory neurons which inhibit the activity of other neurons are central to the propagation of longer spatiotemporal patterns. However, characterizations of connectivity patterns within different classes of inhibitory neurons in the visual cortex (Pfeffer et al., 2013) and electrical and chemical synapses between inhibitory neurons in the cerebellum (Rieubland et al., 2014) have shown that inhibitory neurons can inhibit each other. This could lead to the disinhibition of excitatory neurons that are connected to such populations through overrepresented three neuron motifs, for example I→I→E (Gal et al., 2017; Shimono and Beggs, 2015; Song et al., 2005) along with other motifs such as I→E→I and E→I→I. Recent work on chemogenically induced activation of inhibitory neurons has shown that it suppresses the activity of most interneurons in addition to the suppression of excitatory pyramidal cells (Rogers et al., 2021). Interestingly, a computational model of working memory predicts that enhancing I→I connections would lead to more stable dynamics (Kim and Sejnowski, 2021). This would be consistent with recordings from zebra finches showing that the representation of songs over many days is accompanied by a stable pattern of inhibitory activation, while the population of excitatory neurons is less stable (Liberti et al., 2016). Furthermore, our findings reveal that the proportion of active inhibitory and excitatory neurons in the early stages of neuronal cascades synergistically encodes information about the

duration of such spatiotemporal patterns. This further suggests that inhibitory and excitatory neurons initiate and sustain network dynamics. Future studies can perform more detailed characterizations of connectivity within and across excitatory and inhibitory populations to further tease apart their differential role in regulating network dynamics in neuronal populations.

**Limitations of current work:** Although our findings show that inhibitory neurons within the rich -club play a crucial role in regulating network dynamics, the specific cell morphology of these neurons is not known. Hub neurons in the hippocampus have been found to consist of two types: GABAergic interneurons with long-range axonal projections and basket-like neurons with dense local arborizations (Bonifazi et al., 2009). Interestingly, phasic stimulation of only the basketlike hub neurons led to network synchronization. It was hypothesized that basket cells could act as local hubs whereas long axon projecting hub interneurons could play the role of connector hubs. In the neocortex inhibitory neurons are broadly grouped into PV+, SST and VIP (Tremblay et al., 2016), although recent work has shown that in the visual cortex there are at least 15 different types of inhibitory neurons with distinct morphological and electrophysiological properties (Jiang et al., 2015). Characterizing the morphology of inhibitory hub neurons and examining specific classes of inhibitory neurons within the rich-club will add further insight into how cell type differentially regulates local and long-range network dynamics.

Another potential limitation of this work is that the structural connectivity (synapses, gap junctions) of the neurons from which we record is unknown. Despite impressive technical advances in connectomics, to the best of our knowledge only one group has accomplished a complete reconstruction of a local cortical network using electron microscopy (Turner et al., 2020; Yin et al., 2020); it is much more common to instead provide statistical descriptions (Erö et al., 2018). While it would be extremely desirable to obtain the connectome of such a local cortical circuit, this would not necessarily reveal its dynamics, in the same way that a road map by itself would not definitively indicate traffic flow. A common example in this regard is the case of *C. elegans*, where the connectome has been known for decades (White et al., 1986), yet fruitful work to model how this network routes activity and influences behavior is still revealing surprising new findings (Izquierdo and Lockery, 2010; Luo et al., 2014; Randi and Leifer, 2020). Functional connectivity, like the TE networks we construct here, has proven to be extremely useful at the whole brain level in distinguishing between health and disease (Lynall et al., 2010), conscious and unconscious states (Achard et al., 2012), and networks that have learned from those that have not (Bassett et al., 2011). Given this promising record, we expect that studying functional networks of cortical neurons, like we do here, will be an important step toward identifying microcircuit changes that underlie disease states and learning (Schröter et al., 2017).

**Functional organization of the orbitofrontal cortex:** Our findings implicate a distinct subnetwork (rich-club) with a higher than expected proportion of inhibitory neurons, in regulating network level dynamics in Orbitofrontal cortex (OFC). OFC has been implicated in value based adaptive decision making (Burke et al., 2008; Schoenbaum and Eichenbaum, 1995; Schoenbaum et al., 2009; Wallis, 2012), encoding spatiomotor variables and locomotor actions necessary for achieving behavioral goals (Feierstein et al., 2006) and guiding feeding and social behaviors (Jennings et al., 2019). Recent studies have also shown that OFC dynamically interacts with sensory cortex to guide adaptive behavior (Banerjee et al., 2020). In fact, anatomical studies have shown that OFC shares direct, reciprocal, layer specific connections with primary and secondary visual and auditory areas (Zingg et al., 2014) suggesting its importance in multisensory processing (Sharma and Bandyopadhyay, 2020). However, very little is known about the role of cell-type

specific functional networks in large populations of neurons in OFC that drive such diverse functions (Bissonette et al., 2015; Quirk et al., 2009). Here, by analyzing spontaneous activity from hundreds of neurons in OFC, we have constructed a functional network in large neuronal populations which revealed a specific arrangement of neurons in terms of network topology and cell type composition. Future studies can investigate how this core sub-network of densely connected, inhibition-rich subnetwork drives adaptive behavior during tasks.

**Generality of rich-club architecture:** Prior work has shown that the rich-club topology exists in both the structural and functional organization of the brain at multiple scales and across different species (Betzel et al., 2018; Dann et al., 2016; Harriger et al., 2012; van den Heuvel and Sporns, 2011; Nigam et al., 2016; de Reus and van den Heuvel, 2013; Towlson et al., 2013). At the micro-connectome scale, one important open question is whether functional networks have the same topology across different cortical areas i.e., could our findings in a higher-level associative area like the OFC generalize to sensory areas such as visual, auditory and somatosensory cortex? It is possible that interactions between cell types are driven by the specific function performed by the cortical area as well as its laminar architecture and as a result, network connectivity could be different between sensory and non-sensory areas (Trojanowski et al., 2021). On the other hand, the rich-club may be a general feature of efficient networks. A host of studies in the mouse primary visual cortex (Harris and Mrsic-Flogel, 2013; Ko et al., 2011) has explored the local connectivity patterns between different cell types but the overall network topology at the scale of hundreds of neurons has not been quantified. Detailed anatomical reconstructions of a small volume of the visual cortex have shown the existence of a rich-club topology based on the number of synapses to and from neurons (Gal et al., 2017). However, whether such a structural organization in sensory areas translates to a functional rich-club inferred from spiking activity driven by synaptic strength remains to be seen.

**Implications for cortical models.** Our findings have important implications for cortical network models. Traditionally, these models have used an 80/20 rule for determining the size of excitatory and inhibitory populations. The finding that distinct subnetworks deviate from this excitatory to inhibitory ratio poses the question whether a more compartmental model with different abundances of inhibitory and excitatory neurons and connectivity profiles needs to be implemented. Such models can also provide more detailed understanding of the source and propagation of activity patterns by selectively perturbing different cell types within such networks (Sadeh and Clopath, 2020). Conversely, cortical models could explore what plasticity mechanisms could lead to the formation of an inhibition dominated strongly connected rich-club starting from a randomly connected network topology.

## METHODS

**Data preparation and recording:** All recording procedures were approved by the University of California, Los Angeles, Chancellor's Animal Research Committee. Data was recorded from single housed male mice C57/B1/6J (N = 7, 12-16 weeks old; The Jackson Laboratory) using silicon microprobes as described in a previous study (Shobe et al., 2015). Briefly, extra-cellular activity of hundreds of neurons was recorded simultaneously (sampled at 25 kHz) from awake behaving mice using a 5 shank, 256 site silicon microprobe (50-54 sites per shank arranged in a hexagonal pattern, ~30 µm inter-site spacing, and 300-400 µm inter-shank spacing) inserted into the orbitofrontal cortex. Consecutive microprobes were separated by roughly 0.3 -0.4 mm. Spike sorting was performed offline using a semi-automated Matlab script. The data used for this analysis

were prepared by concatenating resting period activity in between periods when the mouse was performing an odor discrimination task in the same recording session. Resting corresponded to periods of immobility (no treadmill movement and no licking) and a lack of explicitly presented task related stimuli. The firing rates were fairly constant across resting periods except for the last 2 s, where a consistent increase in firing rate was detected. To avoid possible non-stationarities, we deleted the last 2 s from each resting period and then concatenated the different resting periods identified across the entire recording session together to obtain the final spike trains for each recorded neuron.

**Cell-type classification/identification**: Classification of cell types was performed by following methods reported in a recent study (Ren et al., 2020). Briefly, a Gaussian mixture model was fit to features of the extracellularly recorded spike waveforms (Bishop, 2006). This unsupervised clustering method is reasonably accurate, computationally inexpensive, and provides a relatively accurate indicator of cell-type when we do not have access to the ground truth (e.g., from histological analysis on the tissue or optotagging) (Kim et al., 2016; Lima et al., 2009). We have quantified three parameters of the spike waveform that have been proven informative in identifying cell types (Barthó et al., 2004; Sirota et al., 2008; Stark et al., 2013; Trainito et al., 2019): trough-to-peak duration, half amplitude duration and logarithm of firing rate. Trough-to-peak duration is defined as the time interval between the global minimum of the spike waveform and the following local maximum. Half amplitude duration is the duration between the two points where the spike waveform crosses amplitude half the peak. Finally, firing rate is the average number of spikes per second. Although correlated, the first two measures capture different aspects of the intracellular action potential: the speed of depolarization and of the subsequent after-hyperpolarization (Henze et al., 2000) and are both distinguishing features of neuronal cell types (Nowak et al., 2003). Using these three features, we fit the parameters of a 2-component mixture model (means, covariance matrices, and prior probabilities) with Expectation Maximization. We then calculated the posterior probability of each neuron being an excitatory or inhibitory. Here we chose a conservative threshold of 90% likelihood to label neurons as excitatory or inhibitory. Using this threshold, about 97% of neurons are putatively labeled as either excitatory or inhibitory.

**Transfer Entropy analysis:** Transfer Entropy (TE) (Schreiber, 2000) was used to quantify effective connectivity between neurons using the Transfer Entropy Toolbox (Ito et al., 2011) as was described in our previous study (Nigam et al., 2016). TE is an asymmetric information theoretic measure that quantifies causal, non-linear interactions between source and target neurons. TE is non-zero if inclusion of the past activity of the source neuron improves the prediction of the spiking of the target neuron beyond the prediction from the past spiking of the target neuron itself. Briefly, we calculated time lagged TE at a range of delays (1-30ms) between the spiking activity of simultaneously recorded pairs of neurons (source and target). To control for firing rate, we calculated TE between the pairs when the spike times of the target neuron were jittered by 1-19ms drawn from a normal distribution. The mean of the jittered value was then subtracted from the raw estimate between the pairs. Thus, the TE values that remained were directly caused by timing relationships at a resolution less than 20 ms. To control for overall network drive which could lead to increased occurrences of spike coincidences between pairs of neurons, we only considered pairs where TE as a function of time lag had a sharp peak. This was quantified by calculating Coincidence Index (CI) (Ito et al., 2011; Nigam et al., 2016; Shimono and Beggs, 2015) where we evaluated the ratio of the area around the peak (peak time ± 4 ms) to that of the area under the

entire TE vs time lag profile (0-30 ms). Only pairs with both high CI (sharply peaked) and TE were considered for the analysis. The threshold for peak TE and CI was chosen based on TE analysis performed on spiking data generated from a cortical network model where the synaptic connectivity was known beforehand. Values of CI and $TE_{peak}$ that maximized the ratio of true positive rate (TPR) to false positive rate (FPR) for the network model, were used to threshold the effective connectivity estimated from the in-vivo recordings. Finally, possible spurious connections arising out of common drive and transitive drive were eliminated based on analyzing delays at which significant TE was detected in neuronal pairs. This effective connectivity analysis generated sparse, weighted and directed graphs between hundreds of simultaneously recorded neurons.

**Rich-club analysis:** To quantify the strength of connections within neurons in particular subnetworks we used the weighted normalized rich-club coefficient (Colizza et al., 2006; Opsahl et al., 2008) as described in detail in Nigam et al 2016. Briefly, we defined the richness parameter $r$ of each neuron as the sum of the total outgoing and incoming TE from and into that neuron, respectively. Then a list of the unique values of the richness parameter was created, ranked from smallest to largest ($r_{min}$, $r_2$, … $r_{max}$). Additionally, a list of the pairwise TE values ($TE_{rank}$) ranked from largest to smallest was also created ($TE_{max}$, $TE_2$, … $TE_{min}$). Next, we isolated the subnetwork where all neurons had a richness parameter > $r_k$ and counted the number of edges between neurons and defined it as $E_{>r_k}$. We then summed all the pairwise TE values in that subnetwork and defined it to be $W_{>r_k}$. The weighted rich-club coefficient $\Phi^w_{act}$ is the ratio of $W_{>r_k}$ to the sum of the $E_{>r_k}$ strongest pairwise TE values in the network obtained from the list ($TE_{rank}$). This analysis generated weighted rich-club coefficients for each value of the ranked richness parameters ($r_{min}$, $r_2$, … $r_{max}$) defined above. This ratio represents what fraction of the strongest weights in the whole network is present in the subnetwork. To examine whether these coefficients were any different from what would be expected by chance, we used the Brain Connectivity toolbox to generate 1000 randomized versions of the actual networks such that the richness parameters of the neurons were unchanged in each randomized network (Rubinov and Sporns, 2010). We then calculated the weighted rich-club coefficients at the same thresholds from the randomized networks $\Phi^w_{rand}$. The normalized richness coefficient $\Phi^w_{norm}(r_k)$ at each richness parameter was defined as the ratio of $\Phi^w_{act}$ to $\Phi^w_{rand}$. If $\Phi^w_{norm}$ was significantly greater than 1 (Wilcoxon signed rank test; $P < 0.05$) for a range of the richness parameter values, then a rich-club existed in that regime. To correct for multiple comparisons over the range of the richness parameters, false discovery rate (FDR) correction (Benjamini and Yekutieli, 2001) was implemented, limiting the FDR to 0.05.

**Cross-correlation analysis:** We used the Transfer Entropy Toolbox (Ito et al., 2011), to calculate Normalized Cross-Correlation Histogram (NCCH) for pairs of binary spike trains (Brosch and Schreiner, 1999) as follows:

$$NCCH_{raw}(\tau) = \sum \frac{i(t)j(t-\tau)}{\sqrt{n_i n_j}}$$

where $i(t), j(t)$ are the binary states of the neurons at time $t$, i.e., either 1 or 0 based on whether the neurons fired an action potential. $\tau$ is the positive or negative lag in milliseconds at which the state of the second neuron in the pair is evaluated. $n_i$ and $n_j$ are the total number of spikes fired by neuron $i$ and $j$ respectively. The denominator represents the normalization factor which is the

geometric mean of the number of spikes fired by each neuron constituting the pair. Shuffled estimates of NCCH were generated by spike jittering where each spike time was shifted by +/- $t_{shuf}$ drawn randomly from a uniform distribution with 0 mean and a width of 30 ms. The shuffling procedure jittered the temporal pattern of activity of the two neurons but preserved the total number of spikes fired by each neuron. The NCCH values used throughout the analysis were obtained by subtracting the shuffled estimates from the raw values. This correction accounts for correlations arising between spike trains just due to higher firing rates instead of a specific temporal structure at short time scales.

**Synchrony Index (SI):** We defined the Synchrony Index as the area under the shuffle corrected NCCH curve centered at 0 lag and extending to 30 ms on either side (see Figure 2A). Higher values of SI indicate more coincident activity between neuronal pairs within a short time interval and hence more pairwise synchrony. We calculated SI for all pairs of neurons in the data sets and partitioned them into 3 classes: rich-rich, rich-nonrich and nonrich-nonrich based on the membership of the neurons to the rich and non-rich subnetwork. Based on the cell type classification described above we further divided pairs within the rich and non-rich subnetworks into excitatory-excitatory, inhibitory-inhibitory and excitatory-inhibitory pairs and evaluated SI for each of these categories of pairs.

**Population Normalized Population Cross-Correlation (NPCCH):** In order to quantify how the activity of individual neurons influenced the dynamics of specific subnetworks, we calculated the shuffle corrected normalized correlation histogram between the spike train of a reference neuron and all the spikes fired by the rest of the neurons in a defined sub-population (not including the reference neuron). The normalization constant in this case was the geometric mean of the total number of spikes of the reference neuron and that of the sub-population of neurons. Similar to the analysis for pairs, the population measure was evaluated at different positive and negative time lags (-150 ms to +150ms) with respect to each spike of the reference neuron. Raw values of the NPCCH were corrected by subtracting the shuffled estimates obtained by shuffling the spike times of the reference neuron and that of neurons in the subnetwork with the same jitter paradigm used for the pairwise analysis. Area under the NPCCH was evaluated for a pre-period extending from -30 to 0 ms and a post period extending from 0 to +30 ms. 0 ms represents the time point at which the reference neuron fires.

**Granger Causality:** We used Granger Causality (GC) analysis to determine how strongly each subnetwork drove network activity in the other as a function of frequency. Specifically, we generated two new "population" time-series by collecting all the spikes from neurons belonging to each subnetwork respectively. The Akaike information criterion, a principled way to determine the number of time steps included, was then used to calculate the order up to 250 time-bins, and GC was calculated using the, 'multivariate Granger Causality toolbox' (MVGC) (Barnett and Seth, 2014). We calculated shuffled estimates of GC by shifting forward the time series of the source population ten times by one minute increments and the mean of the shuffled estimates was subtracted from the raw values of GC. To calculate GC between two random subnetworks, we randomly sampled two populations size-matched to the rich and non-rich subnetwork respectively 100 times, and calculated shuffle corrected GC between these subnetworks. We then subtracted

the GC estimates for the random subnetworks from the estimates calculated for the actual rich and non-rich subnetworks (GC (actual – random), Figure 3H).

**Cascade dynamics:** In order to identify the role of connectivity and cell types in sustaining and controlling activity in neural circuits, we examined their participation along neuronal cascades. Cascades are defined as consecutive time-bins of neural activity with at least one spike surrounded by two time-bins with no spikes (Figure 4A) and have been reported in both *in-vitro* (Beggs and Plenz, 2003, 2004; Rolston et al., 2007) and *in-vivo* (Hahn et al., 2010; Petermann et al., 2009). We quantify each cascade by its length (CL), i.e., number of time-bins for which it lasts, and its size, i.e., number of unique participating neurons (Figure 4B). To further investigate the role of neurons and their cell type in cascades, we examined the proportion of active inhibitory and excitatory neurons within and outside of the rich-club with respect to all active neurons in every time bin along cascades of different lengths (Figure 4C-F).

**Information theoretic analysis:** Mutual information (MI) and synergy/redundancy was estimated using the Information Breakdown Toolbox (Magri et al., 2009b). The Panzeri-Treves bias correction (Panzeri and Treves, 1996) method implemented in the toolbox was used to account for the bias in mutual information estimation due to limited sampling. In addition to bias correction, we calculated 500 shuffled estimates of MI and ΔI (synergy/redundancy) and these shuffled values were then subtracted from the raw estimates. We calculated the information encoded in the percentage of active excitatory and inhibitory neurons ($Act_{exc}$, $Act_{inh}$) in the first 3 time steps of the cascades (total of 6 factors), about the total length of the cascades ($CL$) using the following expressions,

$$MI(Act, CL) = H(CL) - H(CL|Act) \quad (1)$$

where $H(CL)$ is the entropy in the distribution of cascade lengths and $H(CL|Act)$ represents the conditional entropy given the activation values. Synergy/Redundancy was quantified using the following expression,

$$\Delta I = MI(Act, CL) - MI_{lin} \quad (2)$$

where $MI_{lin}$ is the sum of the mutual information from each factor considered separately. $\Delta I > 0$ implies the joint information is higher than the linear sum of the information provided by each factor, indicating the presence of synergy. If $\Delta I < 0$ implies the joint information is lower than the linear sum of the information provided by each factor, indicating redundancy between the various factors. Finally, if $\Delta I$ is not significantly different from 0, it indicates the joint factors provide as much information about cascade length as the summed information from all the factors separately.

**Quantification and statistical analysis:** We have used non-parametric statistical tests throughout the manuscript as mentioned in the main text. Specifically, for comparing cumulative distributions with different sample sizes we have used the 2-sample KS test. In cases where comparisons were made between 2 distributions with pairwise correspondence, we used the Wilcoxon signed-rank test.

**Data and code availability:** Custom written software used for the analysis reported in this study is available at https://github.com/hadihafizi/InhibRichClubDyn. Information theoretic calculations

were performed using the Information Breakdown toolbox which is available at https://github.com/sunnyneuro/Information_Breakdown_Toolbox.git. Spike data are also available at https://github.com/sotmasman/Cortical-dynamics.

**Acknowledgements:** This work was supported by a Robust Intelligence grant (NSF # 1513779) and IU OVPR bridge funding from Indiana University to JMB, Whitehall Award (ID:1712-114) and IU OVPR Bridge funding from Indiana University to ELN, NIH R01 (grant # 1R01MH121978 to OS and NSF grant (# 1651396) to IHS.

This research was supported in part by Lilly Endowment, inc., through its support for the Indiana University Pervasive Technology Institute. The authors also acknowledge the Indiana University Pervasive Technology Institute for providing supercomputing and storage resources.

**Author contributions:** HH and SN performed the analysis and wrote the manuscript. JB performed granger causality analysis and edited the manuscript. NR and HIS performed cell type classification and edited the manuscript. SCM, OS and ELN edited the manuscript. JMB wrote the manuscript and conceived and supervised the project.

**Competing interests:** The authors declare that they have no competing interests.

## REFERENCES

Achard, S., Delon-Martin, C., Vértes, P.E., Renard, F., Schenck, M., Schneider, F., Heinrich, C., Kremer, S., and Bullmore, E.T. (2012). Hubs of brain functional networks are radically reorganized in comatose patients. Proc. Natl. Acad. Sci. *109*, 20608–20613.

Aguilar-Velázquez, D., and Guzmán-Vargas, L. (2019). Critical synchronization and 1/f noise in inhibitory/excitatory rich-club neural networks. Sci. Rep. *9*, 1–13.

Banerjee, A., Parente, G., Teutsch, J., Lewis, C., Voigt, F.F., and Helmchen, F. (2020). Value-guided remapping of sensory cortex by lateral orbitofrontal cortex. Nature *585*, 245–250.

Barnett, L., and Seth, A.K. (2014). The MVGC multivariate Granger causality toolbox: a new approach to Granger-causal inference. J. Neurosci. Methods *223*, 50–68.

Barthó, P., Hirase, H., Monconduit, L., Zugaro, M., Harris, K.D., and Buzsaki, G. (2004). Characterization of neocortical principal cells and interneurons by network interactions and extracellular features. J. Neurophysiol. *92*, 600–608.

Bassett, D.S., Wymbs, N.F., Porter, M.A., Mucha, P.J., Carlson, J.M., and Grafton, S.T. (2011). Dynamic reconfiguration of human brain networks during learning. Proc. Natl. Acad. Sci. *108*, 7641–7646.

Beggs, J.M., and Plenz, D. (2003). Neuronal avalanches in neocortical circuits. J. Neurosci. *23*, 11167–11177.

Beggs, J.M., and Plenz, D. (2004). Neuronal avalanches are diverse and precise activity patterns that are stable for many hours in cortical slice cultures. J. Neurosci. *24*, 5216–5229.

Benjamini, Y., and Yekutieli, D. (2001). The control of the false discovery rate in multiple

testing under dependency. Ann. Stat. 1165–1188.

Betzel, R.F., Medaglia, J.D., and Bassett, D.S. (2018). Diversity of meso-scale architecture in human and non-human connectomes. Nat. Commun. *9*, 1–14.

Bishop, C.M. (2006). Pattern recognition and machine learning (springer).

Bissonette, G.B., Schoenbaum, G., Roesch, M.R., and Powell, E.M. (2015). Interneurons are necessary for coordinated activity during reversal learning in orbitofrontal cortex. Biol. Psychiatry *77*, 454–464.

Bocchio, M., Gouny, C., Angulo-Garcia, D., Toulat, T., Tressard, T., Quiroli, E., Baude, A., and Cossart, R. (2020). Hippocampal hub neurons maintain distinct connectivity throughout their lifetime. Nat. Commun. *11*, 1–19.

Bonifazi, P., Goldin, M., Picardo, M.A., Jorquera, I., Cattani, A., Bianconi, G., Represa, A., Ben-Ari, Y., and Cossart, R. (2009). GABAergic hub neurons orchestrate synchrony in developing hippocampal networks. Science. *326*, 1419–1424.

Bosman, C.A., Schoffelen, J.-M., Brunet, N., Oostenveld, R., Bastos, A.M., Womelsdorf, T., Rubehn, B., Stieglitz, T., De Weerd, P., and Fries, P. (2012). Attentional stimulus selection through selective synchronization between monkey visual areas. Neuron *75*, 875–888.

Brosch, M., and Schreiner, C.E. (1999). Correlations between neural discharges are related to receptive field properties in cat primary auditory cortex. Eur. J. Neurosci. *11*, 3517–3530.

Burke, K.A., Franz, T.M., Miller, D.N., and Schoenbaum, G. (2008). The role of the orbitofrontal cortex in the pursuit of happiness and more specific rewards. Nature *454*, 340–344.

Bush, P., and Sejnowski, T. (1996). Inhibition synchronizes sparsely connected cortical neurons within and between columns in realistic network models. J. Comput. Neurosci. *3*, 91–110.

Chambers, B., and MacLean, J.N. (2016). Higher-order synaptic interactions coordinate dynamics in recurrent networks. PLoS Comput. Biol. *12*, e1005078.

Cho, K.K.A., Davidson, T.J., Bouvier, G., Marshall, J.D., Schnitzer, M.J., and Sohal, V.S. (2020). Cross-hemispheric gamma synchrony between prefrontal parvalbumin interneurons supports behavioral adaptation during rule shift learning. Nat. Neurosci. 1–11.

Colizza, V., Flammini, A., Serrano, M.A., and Vespignani, A. (2006). Detecting rich-club ordering in complex networks. Nat. Phys. 2, 110-115.

Dann, B., Michaels, J.A., Schaffelhofer, S., and Scherberger, H. (2016). Uniting functional network topology and oscillations in the fronto-parietal single unit network of behaving primates. Elife *5*, e15719.

Douglas, R.J., and Martin, K.A.C. (2004). Neuronal circuits of the neocortex. Annu. Rev. Neurosci. *27*, 419–451.

English, D.F., McKenzie, S., Evans, T., Kim, K., Yoon, E., and Buzsáki, G. (2017). Pyramidal cell-interneuron circuit architecture and dynamics in hippocampal networks. Neuron *96*, 505–520.

Erö, C., Gewaltig, M.-O., Keller, D., and Markram, H. (2018). A cell atlas for the mouse brain. Front. Neuroinform. *12*, 84.

Faber, S.P., Timme, N.M., Beggs, J.M., and Newman, E.L. (2019). Computation is concentrated in rich clubs of local cortical networks. Netw. Neurosci. *3*, 384–404.

Feierstein, C.E., Quirk, M.C., Uchida, N., Sosulski, D.L., and Mainen, Z.F. (2006). Representation of spatial goals in rat orbitofrontal cortex. Neuron *51*, 495–507.

Fries, P. (2005). A mechanism for cognitive dynamics: neuronal communication through neuronal coherence. Trends Cogn. Sci. *9*, 474–480.

Gal, E., London, M., Globerson, A., Ramaswamy, S., Reimann, M.W., Muller, E., Markram, H., and Segev, I. (2017). Rich cell-type-specific network topology in neocortical microcircuitry. Nat. Neurosci. *20*, 1004.

Gu, Y., Qi, Y., and Gong, P. (2019). Rich-club connectivity, diverse population coupling, and dynamical activity patterns emerging from local cortical circuits. PLoS Comput. Biol. *15*, e1006902.

Hafizi, M.H. (2020). Rich Club, Inhibition and Network Dynamics in the Cortical Microconnectome.

Hagmann, P., Cammoun, L., Gigandet, X., Meuli, R., Honey, C.J., Wedeen, V.J., and Sporns, O. (2008). Mapping the structural core of human cerebral cortex. PLoS Biol *6*, e159.

Hahn, G., Petermann, T., Havenith, M.N., Yu, S., Singer, W., Plenz, D., and Nikolić, D. (2010). Neuronal avalanches in spontaneous activity in vivo. J. Neurophysiol. *104*, 3312–3322.

Harriger, L., Van Den Heuvel, M.P., and Sporns, O. (2012). Rich club organization of macaque cerebral cortex and its role in network communication. PLoS One *7*, e46497.

Harris, K.D., and Mrsic-Flogel, T.D. (2013). Cortical connectivity and sensory coding. Nature *503*, 51–58.

Hasenstaub, A., Shu, Y., Haider, B., Kraushaar, U., Duque, A., and McCormick, D.A. (2005). Inhibitory postsynaptic potentials carry synchronized frequency information in active cortical networks. Neuron *47*, 423–435.

Henze, D.A., Borhegyi, Z., Csicsvari, J., Mamiya, A., Harris, K.D., and Buzsaki, G. (2000). Intracellular features predicted by extracellular recordings in the hippocampus in vivo. J. Neurophysiol. *84*, 390–400.

van den Heuvel, M.P., and Sporns, O. (2011). Rich-club organization of the human connectome. J. Neurosci.

Ito, S., Hansen, M.E., Heiland, R., Lumsdaine, A., Litke, A.M., and Beggs, J.M. (2011). Extending transfer entropy improves identification of effective connectivity in a spiking cortical network model. PLoS One *6*, e27431.

Izquierdo, E.J., and Lockery, S.R. (2010). Evolution and analysis of minimal neural circuits for klinotaxis in Caenorhabditis elegans. J. Neurosci. *30*, 12908–12917.

Jennings, J.H., Kim, C.K., Marshel, J.H., Raffiee, M., Ye, L., Quirin, S., Pak, S., Ramakrishnan, C., and Deisseroth, K. (2019). Interacting neural ensembles in orbitofrontal cortex for social and feeding behaviour. Nature *565*, 645–649.

Jiang, X., Shen, S., Cadwell, C.R., Berens, P., Sinz, F., Ecker, A.S., Patel, S., and Tolias, A.S. (2015). Principles of connectivity among morphologically defined cell types in adult neocortex. Science. *350(6264)*.

Kajiwara, M., Nomura, R., Goetze, F., Kawabata, M., Isomura, Y., Akutsu, T., and Shimono, M. (2021). Inhibitory neurons exhibit high controlling ability in the cortical microconnectome. PLOS Comput. Biol. *17*, e1008846.

Kim, R., and Sejnowski, T.J. (2021). Strong inhibitory signaling underlies stable temporal dynamics and working memory in spiking neural networks. Nat. Neurosci. *24*, 129–139.

Kim, D., Jeong, H., Lee, J., Ghim, J.-W., Her, E.S., Lee, S.-H., and Jung, M.W. (2016). Distinct roles of parvalbumin-and somatostatin-expressing interneurons in working memory. Neuron *92*, 902–915.

Ko, H., Hofer, S.B., Pichler, B., Buchanan, K.A., Sjöström, P.J., and Mrsic-Flogel, T.D. (2011). Functional specificity of local synaptic connections in neocortical networks. Nature *473*, 87–91.

Liberti, W.A., Markowitz, J.E., Perkins, L.N., Liberti, D.C., Leman, D.P., Guitchounts, G., Velho, T., Kotton, D.N., Lois, C., and Gardner, T.J. (2016). Unstable neurons underlie a stable learned behavior. Nat. Neurosci. *19*, 1665–1671.

Lima, S.Q., Hromádka, T., Znamenskiy, P., and Zador, A.M. (2009). PINP: a new method of tagging neuronal populations for identification during in vivo electrophysiological recording. PLoS One *4*, e6099.

Luo, L., Wen, Q., Ren, J., Hendricks, M., Gershow, M., Qin, Y., Greenwood, J., Soucy, E.R., Klein, M., and Smith-Parker, H.K. (2014). Dynamic encoding of perception, memory, and movement in a C. elegans chemotaxis circuit. Neuron *82*, 1115–1128.

Lynall, M.-E., Bassett, D.S., Kerwin, R., McKenna, P.J., Kitzbichler, M., Muller, U., and Bullmore, E. (2010). Functional connectivity and brain networks in schizophrenia. J. Neurosci. *30*, 9477–9487.

Magri, C., Whittingstall, K., Singh, V., Logothetis, N.K., and Panzeri, S. (2009a). A toolbox for the fast information analysis of multiple-site LFP, EEG and spike train recordings. BMC Neurosci. *10*, 1–24.

Magri, C., Whittingstall, K., Singh, V., Logothetis, N.K., and Panzeri, S. (2009b). A toolbox for the fast information analysis of multiple-site LFP, EEG and spike train recordings. BMC Neurosci. *10*.

Markov, N.T., Ercsey-Ravasz, M., Van Essen, D.C., Knoblauch, K., Toroczkai, Z., and Kennedy, H. (2013). Cortical high-density counterstream architectures. Science. *342(6158)*.

Modol, L., Bollmann, Y., Tressard, T., Baude, A., Che, A., Duan, Z.R.S., Babij, R., García, N.V.D.M., and Cossart, R. (2020). Assemblies of perisomatic GABAergic neurons in the developing barrel cortex. Neuron *105*, 93–105.

Nigam, S., Shimono, M., Ito, S., Yeh, F.-C., Timme, N., Myroshnychenko, M., Lapish, C.C., Tosi, Z., Hottowy, P., Smith, W.C., et al. (2016). Rich-club organization in effective connectivity among cortical neurons. J. Neurosci. *36(3), 670-684*.

Nigam, S., Pojoga, S., and Dragoi, V. (2019). Synergistic Coding of Visual Information in Columnar Networks. Neuron *104(2), 402-411*.

Nowak, L.G., Azouz, R., Sanchez-Vives, M. V, Gray, C.M., and McCormick, D.A. (2003). Electrophysiological classes of cat primary visual cortical neurons in vivo as revealed by quantitative analyses. J. Neurophysiol. *89*, 1541–1566.

Opsahl, T., Colizza, V., Panzarasa, P., and Ramasco, J.J. (2008). Prominence and control: the weighted rich-club effect. Phys. Rev. Lett. *101*, 168702.

Panzeri, S., and Treves, A. (1996). Analytical estimates of limited sampling biases in different information measures. Netw. Comput. Neural Syst. *7*, 87–107.

Petermann, T., Thiagarajan, T.C., Lebedev, M.A., Nicolelis, M.A.L., Chialvo, D.R., and Plenz, D. (2009). Spontaneous cortical activity in awake monkeys composed of neuronal avalanches. Proc. Natl. Acad. Sci. *106*, 15921–15926.

Pfeffer, C.K., Xue, M., He, M., Huang, Z.J., and Scanziani, M. (2013). Inhibition of inhibition in visual cortex: the logic of connections between molecularly distinct interneurons. Nat. Neurosci. *16*, 1068–1076.

Picardo, M.A., Guigue, P., Bonifazi, P., Batista-Brito, R., Allene, C., Ribas, A., Fishell, G., Baude, A., and Cossart, R. (2011). Pioneer GABA cells comprise a subpopulation of hub neurons in the developing hippocampus. Neuron *71*, 695–709.

Quirk, M.C., Sosulski, D.L., Feierstein, C.E., Uchida, N., and Mainen, Z.F. (2009). A defined network of fast-spiking interneurons in orbitofrontal cortex: responses to behavioral contingencies and ketamine administration. Front. Syst. Neurosci. *3*, 13.

Randi, F., and Leifer, A.M. (2020). Measuring and modeling whole-brain neural dynamics in Caenorhabditis elegans. Curr. Opin. Neurobiol. *65*, 167–175.

Ren, N., Ito, S., Hafizi, H., Beggs, J.M., and Stevenson, I.H. (2020). Model-based detection of putative synaptic connections from spike recordings with latency and type constraints. J. Neurophysiol. *124*, 1588–1604.

de Reus, M.A., and van den Heuvel, M.P. (2013). Rich club organization and intermodule communication in the cat connectome. J. Neurosci. *33*, 12929–12939.

Rieubland, S., Roth, A., and Häusser, M. (2014). Structured connectivity in cerebellar inhibitory networks. Neuron *81*, 913–929.

Rogers, S., Rozman, P.A., Valero, M., Doyle, W.K., and Buzsáki, G. (2021). Mechanisms and plasticity of chemogenically induced interneuronal suppression of principal cells. Proc. Natl. Acad. Sci. *118(2)*.

Rolston, J.D., Wagenaar, D.A., and Potter, S.M. (2007). Precisely timed spatiotemporal patterns of neural activity in dissociated cortical cultures. Neuroscience *148*, 294–303.

Rubinov, M., and Sporns, O. (2010). Complex network measures of brain connectivity: uses and interpretations. Neuroimage *52*, 1059–1069.

Sadeh, S., and Clopath, C. (2020). Theory of neuronal perturbome in cortical networks. Proc. Natl. Acad. Sci. *117*, 26966–26976.

Schoenbaum, G., and Eichenbaum, H. (1995). Information coding in the rodent prefrontal cortex. I. Single-neuron activity in orbitofrontal cortex compared with that in pyriform cortex. J. Neurophysiol. *74*, 733–750.

Schoenbaum, G., Roesch, M.R., Stalnaker, T.A., and Takahashi, Y.K. (2009). A new perspective on the role of the orbitofrontal cortex in adaptive behaviour. Nat. Rev. Neurosci. *10*, 885–892.

Schreiber, T. (2000). Measuring information transfer. Phys. Rev. Lett. *85*, 461.

Schröter, M., Paulsen, O., and Bullmore, E.T. (2017). Micro-connectomics: probing the organization of neuronal networks at the cellular scale. Nat. Rev. Neurosci. *18*, 131.

Sharma, S., and Bandyopadhyay, S. (2020). Differential rapid plasticity in auditory and visual responses in the primarily multisensory orbitofrontal cortex. Eneuro *7(3)*.

Shimono, M., and Beggs, J.M. (2015). Functional clusters, hubs, and communities in the cortical microconnectome. Cereb. Cortex *25*, 3743–3757.

Shobe, J.L., Claar, L.D., Parhami, S., Bakhurin, K.I., and Masmanidis, S.C. (2015). Brain activity mapping at multiple scales with silicon microprobes containing 1,024 electrodes. J. Neurophysiol. *114*, 2043–2052.

Sirota, A., Montgomery, S., Fujisawa, S., Isomura, Y., Zugaro, M., and Buzsáki, G. (2008). Entrainment of neocortical neurons and gamma oscillations by the hippocampal theta rhythm. Neuron *60*, 683–697.

Song, S., Sjöström, P.J., Reigl, M., Nelson, S., and Chklovskii, D.B. (2005). Highly nonrandom features of synaptic connectivity in local cortical circuits. PLoS Biol *3(3)*, e68.

Stark, E., Eichler, R., Roux, L., Fujisawa, S., Rotstein, H.G., and Buzsáki, G. (2013). Inhibition-induced theta resonance in cortical circuits. Neuron *80*, 1263–1276.

Tort, A.B.L., Rotstein, H.G., Dugladze, T., Gloveli, T., and Kopell, N.J. (2007). On the formation of gamma-coherent cell assemblies by oriens lacunosum-moleculare interneurons in the hippocampus. Proc. Natl. Acad. Sci. *104*, 13490–13495.

Towlson, E.K., Vértes, P.E., Ahnert, S.E., Schafer, W.R., and Bullmore, E.T. (2013). The rich club of the C. elegans neuronal connectome. J. Neurosci. *33*, 6380–6387.

Trainito, C., von Nicolai, C., Miller, E.K., and Siegel, M. (2019). Extracellular spike waveform dissociates four functionally distinct cell classes in primate cortex. Curr. Biol. *29*, 2973–2982.

Tremblay, R., Lee, S., and Rudy, B. (2016). GABAergic interneurons in the neocortex: from cellular properties to circuits. Neuron *91*, 260–292.

Trojanowski, N.F., Bottorff, J., and Turrigiano, G.G. (2021). Activity labeling in vivo using CaMPARI2 reveals intrinsic and synaptic differences between neurons with high and low firing

rate set points. Neuron *109*, 663–676.

Turner, N.L., Macrina, T., Bae, J.A., Yang, R., Wilson, A.M., Schneider-Mizell, C., Lee, K., Lu, R., Wu, J., and Bodor, A.L. (2020). Multiscale and multimodal reconstruction of cortical structure and function. BioRxiv.

Van Vreeswijk, C., Abbott, L.F., and Ermentrout, G.B. (1994). When inhibition not excitation synchronizes neural firing. J. Comput. Neurosci. *1*, 313–321.

Wallis, J.D. (2012). Cross-species studies of orbitofrontal cortex and value-based decision-making. Nat. Neurosci. *15*, 13–19.

White, J.G., Southgate, E., Thomson, J.N., and Brenner, S. (1986). The structure of the nervous system of the nematode Caenorhabditis elegans. Philos Trans R Soc L. B Biol Sci *314*, 1–340.

Womelsdorf, T., Schoffelen, J.-M., Oostenveld, R., Singer, W., Desimone, R., Engel, A.K., and Fries, P. (2007). Modulation of neuronal interactions through neuronal synchronization. Science. *316*, 1609–1612.

Yin, W., Brittain, D., Borseth, J., Scott, M.E., Williams, D., Perkins, J., Own, C.S., Murfitt, M., Torres, R.M., and Kapner, D. (2020). A petascale automated imaging pipeline for mapping neuronal circuits with high-throughput transmission electron microscopy. Nat. Commun. *11*, 1–12.

Zingg, B., Hintiryan, H., Gou, L., Song, M.Y., Bay, M., Bienkowski, M.S., Foster, N.N., Yamashita, S., Bowman, I., and Toga, A.W. (2014). Neural networks of the mouse neocortex. Cell *156*, 1096–1111.

**Supplemental information**

# Inhibition-Dominated Rich-Club Shapes Dynamics in Cortical Microcircuits in Awake Behaving Mice

Hadi Hafizi, Sunny Nigam, Josh Barnathan, Naixin Ren, Ian H Stevenson, Sotiris C Masmanidis, Ehren L Newman, Olaf Sporns, and John M Beggs.

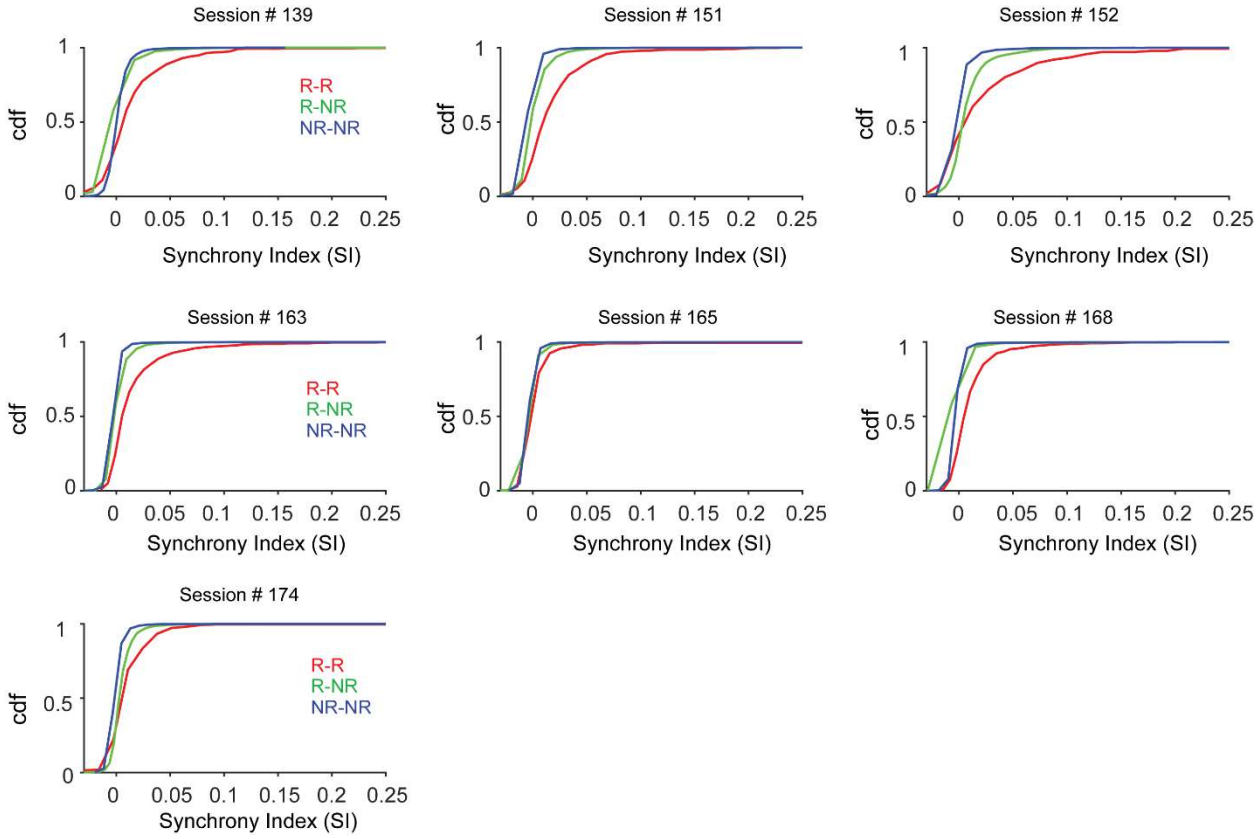


**Figure S1.** Cumulative distribution of Synchrony Index (SI) for each of the 7 sessions. Red, green and blue curves represent cumulative distributions of SI evaluated for pairs within the rich-club, non-rich subnetwork and pairs with mixed membership (rich and non-rich) respectively.

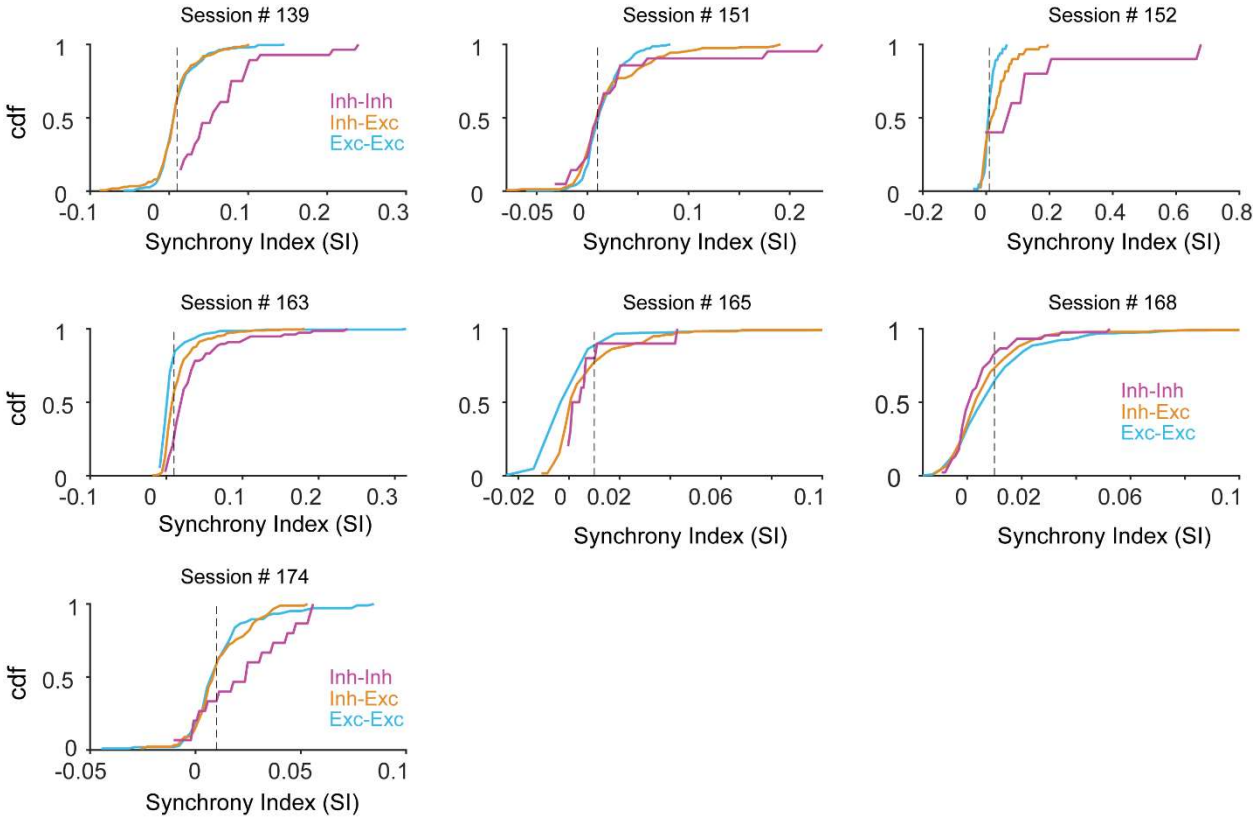


**Figure S2.** Cumulative distribution of Synchrony Index (SI) for different classes of pairs within the rich-club in each of the 7 sessions. Purple, orange and cyan curves represent cumulative distributions of SI evaluated for inhibitory-inhibitory, inhibitory-excitatory and excitatory-excitatory pairs within the rich-club. Dotted vertical line shows SI = 0.01.

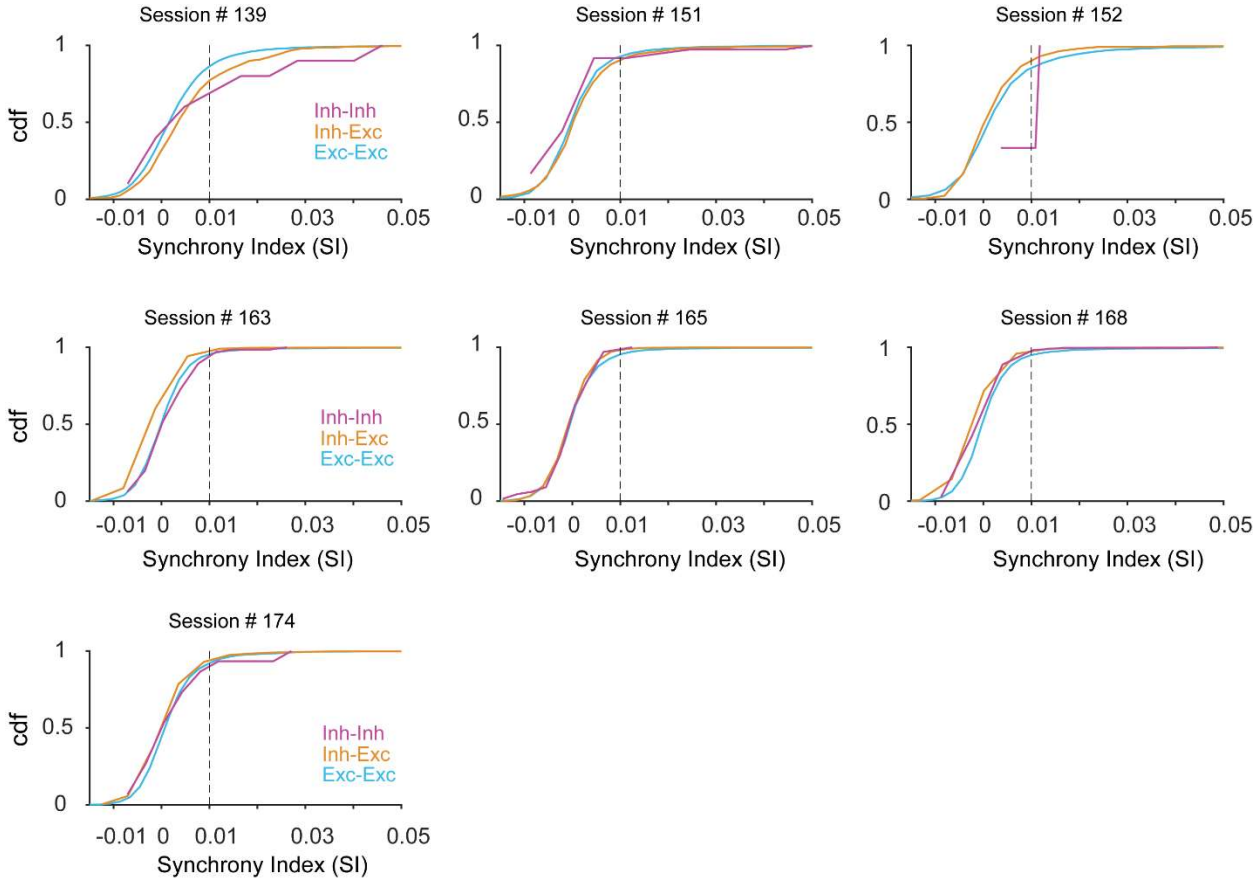


**Figure S3.** Cumulative distribution of Synchrony Index (SI) for different classes of pairs within the non-rich subnetwork in each of the 7 sessions. Purple, orange and cyan curves represent cumulative distributions of SI evaluated for inhibitory-inhibitory, inhibitory-excitatory and excitatory-excitatory pairs within the non-rich subnetwork. Dotted vertical line shows SI = 0.01.

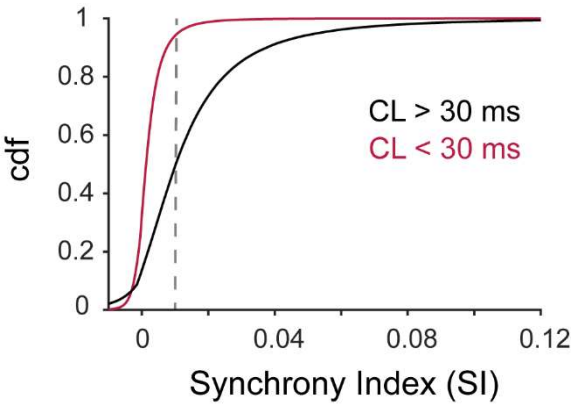


**Figure S4.** Cumulative distribution of Synchrony Index evaluated for neurons participating in cascade lengths (CL) > 30 ms (black) and CL < 30 ms (red) pooled across N = 7 sessions. Dotted line shows SI value of 0.01. Note significantly higher SI values (> 0.01) for longer cascade lengths compared to shorter ones (2-sample KS test; $P < 0.001$).